



High-pressure structural, lattice dynamics, and electronic properties of beryllium aluminate studied from first-principles theory

Jaspreet Singh^a, Vineet Kumar Sharma^a, V. Kanchana^{a,*}, G. Vaitheeswaran^b, D. Errandonea^c

^a Department of Physics, Indian Institute of Technology Hyderabad, Kandi-502285, Sangareddy, Telangana, India

^b School of Physics, University of Hyderabad, Prof. C. R. Rao Road, Gachibowli, Hyderabad, 500 046 Telangana, India

^c Departamento de Física Aplicada-ICMUV-MALTA Consolider Team, Universidad de Valencia, C/Dr. Moliner 50, 46100, Burjassot, Valencia, Spain

ARTICLE INFO

Keywords:

The structural properties
Thermodynamic properties
Optical isotropy
Band gap
Phonons

ABSTRACT

The present work reports the complete study of structural, vibrational, mechanical, and electronic properties of BeAl_2O_4 (known as Chrysoberyl) using first-principles computing methods. The calculated ground-state properties agree quite well with previous experiments. The computed phonon dispersion curves do not show imaginary frequencies confirming the dynamical stability. In addition, the calculated elastic constants also ensure the mechanical stability through fulfillment of mechanical stability criteria. Apart from that, the theoretically determined phonon frequencies agree quite well with previous Raman and infrared experiments at ambient conditions. Various thermodynamic properties are also being calculated as a function of temperature. The thermal expansion computed within the quasi-harmonic approximation is found to be positive in agreement with the experiments. From the electronic structure we can see that Chrysoberyl possess a direct band gap of 8.3 eV with the oxygen- $2p$ states dominating close to fermi level in the valence band. The influence of pressure on different properties is discussed. The highlight of the present work is the presence of optical isotropy in Chrysoberyl although the crystal structure is highly anisotropic.

1. Introduction

In 1926, Bragg and Brown had reported the crystal structure of Olivine, the primary component of the Earth's upper mantle. Isomorphous structures are shared by several minerals, which constitute the Olivine family. Alexandrite, Sinhalite, Peridot, Forsterite, and Chrysoberyl are among them. The minerals of the Olivine series have orthorhombic crystal symmetry being their crystal structure described by space group $Pbnm$ (No. 62) [1]. The structure of Chrysoberyl (BeAl_2O_4) was refined by Farrell and coworkers in 1963. It is composed of tetrahedral BeO_4 groups and octahedral AlO_6 units [2]. After Diamond and Corundum, Chrysoberyl is the third hardest gemstone. When doped with Cr^{3+} is known as Alexandrite, having multiple technological applications, which include the use as high-temperature sensor [3], as phosphor material [4], and as active-media in lasers [5]. The crystal structure of BeAl_2O_4 is closely related to the Spinel structure of many aluminates in terms of chemical composition, but it has a crystal structure isomorphous to the Olivine-type structures as discussed above. The structural arrangement similar to that of Spinel MgAl_2O_4 has been used to claim BeAl_2O_4 as Spinel [6,7]. However, the most recent crystallographic studies have

undoubtedly identified the crystal structure as Olivine-type [8]. Chrysoberyl and its Cr^{3+} -doped variety Alexandrite can be obtained synthetically as high-quality single crystals, showing Alexandrite an excellent laser behavior [9]. The improvement of the knowledge of the properties of BeAl_2O_4 would contribute to the improvement of its many practical applications.

Mostly Be-minerals belong to the system $\text{BeO-Al}_2\text{O}_3\text{-SiO}_2\text{-H}_2\text{O}$ (BASH). There are more than twenty phases, which exist in this BASH system. At $\sim 1500^\circ\text{C}$, three crystalline phases namely, Chrysoberyl, Phenacite, and Cristobalite were found at co-existing state in the high-silica region of the $\text{BeO-Al}_2\text{O}_3\text{-SiO}_2$ system [10]. Beryl, Chrysoberyl, Phenacite, Bromellite, Bertrandite, Mullite, Quartz, Pyrophyllite, and Kaolinite phases were found from the system BASH. It has been also reported Chrysoberyl could coexist with many of the other mentioned minerals, in particular with Beryl [11]. The fact that Chrysoberyl (BeAl_2O_4) is an Olivine isomorph crystal make its study of interest for Earth Sciences. In particular, from the view of geochemistry, Olivines are very interesting materials for features such as low compressibility, high-wave velocities, and high elastic ratio [12]. Olivine silicates are some of the most elastically anisotropic minerals, with wave velocities

* Corresponding author.

E-mail address: kanchana@iith.ac.in (K. V.).

<https://doi.org/10.1016/j.mtcomm.2020.101801>

Received 24 August 2020; Received in revised form 22 October 2020; Accepted 22 October 2020

Available online 4 November 2020

2352-4928/© 2020 Elsevier Ltd. All rights reserved.

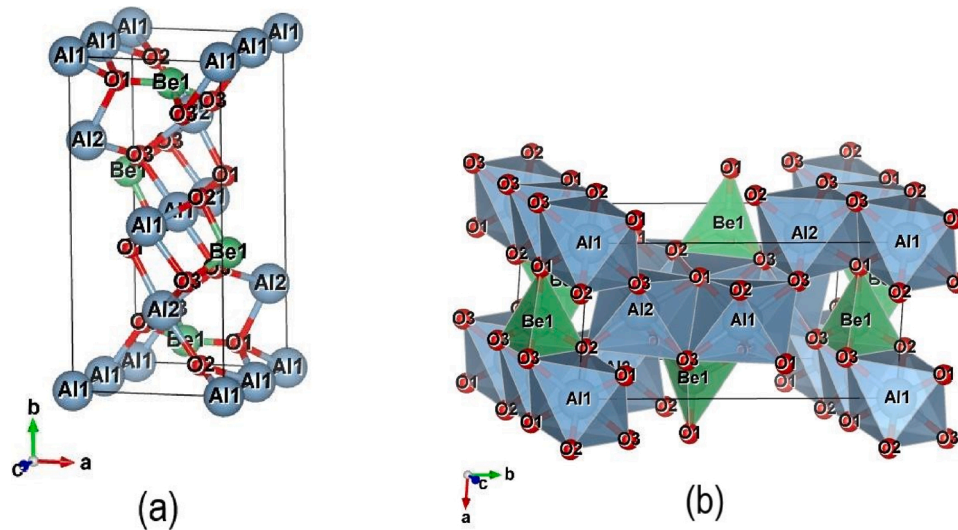


Fig. 1. Crystal structure of BeAl_2O_4 .

along a crystallographic axis greater than along b and c i.e. $v_a > v_c > v_b$. The order of wave velocities is opposite to that of thermal expansion coefficients and of linear compressibility coefficients. In particular, wave velocities or compressional velocities along a axis is almost 30 % larger than that along b axis. Olivine silicates also show anisotropies on the elastic constants being: $C_{11} > C_{33} > C_{22}$ [12,13].

Most physical properties of minerals depend upon pressure and temperature. Thermal expansion, compressibility, conductivity, etc. are drastically altered when subjected to pressure and temperature and the investigation about the minerals at high temperatures and high pressures is certainly an inevitable requirement in science. Many high-temperature studies have been done on the Olivine crystals. Several investigators have determined the thermal expansion curves of the Olivines [14–16]. To investigate the anisotropic compression in Olivines, high-pressure studies have been done on Forsterite, Fayalite, and Monticellite [16–20]. Physical properties of solids depend on the atomic arrangement. On applying temperature and pressure, the variation occurs in the atomic position and their physical properties changes. Olivine has two octahedral sites and one tetrahedral site and three distinguishable oxygen positions. Ions located at octahedral sites are having different symmetry i.e. $M(1)$ site has inversion symmetry and $M(2)$ has mirror symmetry. Both sites have different bond length with oxygen. $M(2)$ has a larger bond length than $M(1)$ [21]. Forsterite under high pressure and high temperature was well investigated. In Forsterite, octahedral distortion increases with the increase in temperature, but it does not vary significantly with increasing pressure. It is found that temperature and pressure have greater effect on large Mg-O bonds than the short Mg-O bonds [16]. In addition to Olivine-type compounds, Spinel-type aluminates have been broadly studied under high-pressure conditions [22,23]. The same can be stated for Sinhalite [24]. In contrast with the minerals and compounds described above, BeAl_2O_4 has been much less studied. The structural properties have studied under compression by x-ray diffraction only up to 6.5 GPa [25]. In subsequent studies, Ching et al. [26] discussed the spectroscopic properties of BeAl_2O_4 at ambient conditions and reported the bulk modulus, and Jahren et al. investigated the behavior of fluorescence under high-pressure in Cr-doped BeAl_2O_4 [27]. The fracture toughness and surface energies of minerals including BeAl_2O_4 were reported using ionic crystal model [28]. Another recent density functional theory calculation based on linear combination of atomic orbitals addressing the structural and electronic properties of several Spinel-type oxides (which includes BeAl_2O_4), sulphides were also reported [29]. For nearly two decades, nothing has been done on BeAl_2O_4 under high-pressure conditions. This motivated us to explore the ground state, electronic

structure and vibrational properties of this aluminate both at ambient and at high pressure, which we have performed using the ab-initio density-functional calculations, an efficient tool to study the properties of ternary oxides [30].

In our present study, we will explore the different physical properties of BeAl_2O_4 and the influence of pressure and temperature in $P-T$ ranges of interest for technological applications of BeAl_2O_4 . We characterize the structural aspects and outline the computational details of BeAl_2O_4 in section II. Section III describes the main results and discussion on the structural properties, elastic and mechanical properties, dynamical properties, thermodynamic properties, electronic structure properties and optical properties. We discuss the structural, elastic and mechanical properties and electronic structure properties at ambient as well as under pressure. In the last section IV, we briefly outline the conclusions.

2. Computational details and structural aspects

The geometry optimization has been carried out using the Projector-Augmented Wave (PAW) method as implemented in VASP within the framework of DFT (density-functional theory) [31]. The Perdew-Burke-Ernzerhof (PBE) potentials within the Generalized-Gradient Approximation (GGA) were used for the exchange correlation functionals [32]. The plane wave energy cutoff was set to 520 eV for all calculations. The energy convergence criteria have been chosen to be 10^{-6} eV. According to the Monkhorst-Pack scheme, a $10 \times 5 \times 8$ k-mesh has been used for the geometry optimization calculations [33]. The density-functional perturbation theory using VASP with combination of Phonopy has been used to perform phonon-dispersion calculations [34]. ELATE software has been used for three- and two-dimensional Young modulus plotting [35]. The thermodynamic properties of the investigated system have been calculated under the Quasi-Harmonic approximation using the combination of VASP and Phonopy [36]. The converged output from VASP has been taken as an input to perform the electronic-structure properties in Wien2k. Due to the underestimation of GGA approximation in calculating the band gap of semiconductors/insulators [37], the electronic properties of BeAl_2O_4 have been computed using a semi-empirical Tran and Blaha modification of the Becke-Johnson (TB-mBJ) functional in the self-consistent FP-LAPW (full-potential linear augmented plane wave) method as implemented in Wien2k [38]. To see the band gap variation as a function of pressure, calculations were carried out by VASP with PBE-GGA potentials. The vibrational properties are computed using the CASTEP code [39] within the framework of density-functional perturbation

Table 1

Unit-cell parameters and bond distances (Å). Calculated results from this work are compared with experiments [25]. The multiplicity of bonds is indicated (e.g. as x 2). The numbers in the parentheses represent *esd*'s.

	Experimental	Calculated
<i>a</i> (Å)	4.428 (1)	4.464
<i>b</i> (Å)	9.415 (3)	9.500
<i>c</i> (Å)	5.481 (2)	5.529
<i>V</i> (Å ³)	228.5 (1)	234.48
Al1-O	1.863 × 2 (2), 1.893 × 2 (2), 1.911 × 2 (2)	1.8856 × 2, 1.9104 × 2, 1.9308 × 2
Al2-O	1.864 (3), 1.894 × 2 (2), 1.940 (3), 2.020 × 2 (2)	1.8798, 1.9119 × 2, 1.9654, 2.0343 × 2
Be-O	1.581 (7), 1.641 × 2 (4), 1.694 (6)	1.5790, 1.6550 × 2, 1.6985

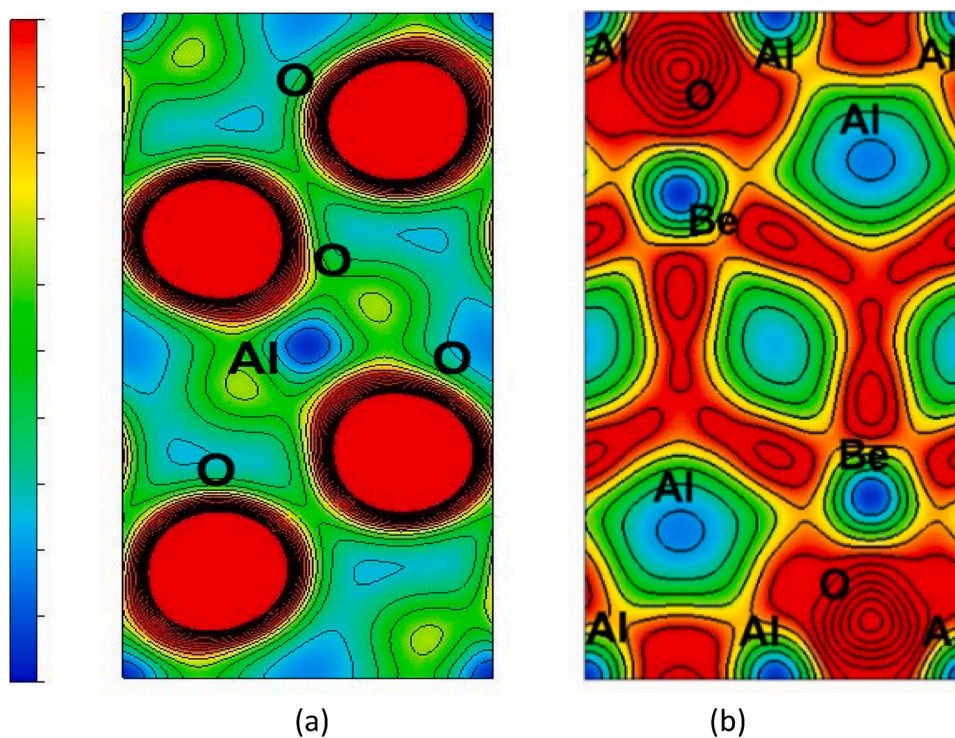


Fig. 2. Charge density along (100) plane in BeAl_2O_4 . The contour lines range from 0.00 to 0.25 electrons/(a.u.)³ in intervals of 0.005. (a) $z = 0.3$ plane (b) $z = 0$ plane. Color bar depicts the maximum and minimum charge density by red and blue colors respectively (For interpretation of the references to colour in this figure legend, the reader is referred to the web version of this article).

theory.

To describe the behavior of the unit-cell volume under compression, the bulk modulus and its pressure derivative, were determined for BeAl_2O_4 by fitting the pressure-volume ($P - V$) results to a third order Birch-Murnaghan equation of state (EOS) [40].

3. Results and discussions

3.1. Structural properties

As mentioned in the introduction, BeAl_2O_4 is closely related to Olivine-type and also possess similarity with the Spinel-type mineral. The crystallographic isomorphism with Olivine-type structures intends us to explored this form which is described with space group $Pbnm$. The crystal structure is schematically shown in Fig. 1. According to previous studies, the lattice parameters at ambient conditions are $a = 4.428$ Å, $b = 9.415$ Å, and $c = 5.481$ Å [25]. Our calculations describe very accurately the crystal structure of the studied aluminate, which can be seen from Table 1. In particular, the calculated unit-cell parameters show the agreement with experiments within 1%.

In the crystal structure of BeAl_2O_4 , there are two non-equivalent Al

sites, one of them is a mirror site and another is an inversion site and three O sites. The mirror site is preferred for the substitution of Cr or Fe ions [41]. There are hexagonal close-packed oxygen atoms in the structure with aluminum and beryllium atoms octahedrally and tetrahedrally coordinated, respectively. All oxygen atoms bond to one beryllium and three aluminum ions. Oxygen ions (except O3) are having same bonding with Be and Al ions. O1 and O2 each bond to one Be, two Al1 and one Al2, while O3 bonds to one Be, one Al1 and two Al2. Both AlO_6 octahedra have Al-O bond distances ranging from 1.885 to 2.034 Å. On the other hand, BeO_4 tetrahedral units have relatively short Be-O bond distances of 1.579, 1.655 (x2), and 1.698 Å. The calculated bond distances are listed in Table 1, which is agree with the experiments. Excellent agreement is also obtained for the atomic positions as can be seen in Table S1 (supplementary material). In addition, the charge density also is being plotted along (100) plane, which are shown in Fig. 2. From the plots, it is observed that the charge is mostly localized around O atoms as it is more electronegative than both Al and Be atoms. The color bar depicts the difference in charge density localized (red color) and flowing charge (blue color). The localized charge around the O atom is sign of gaining of charge and shape of O atom is not spherical, corresponds to covalent nature. Our results are consistent with reported

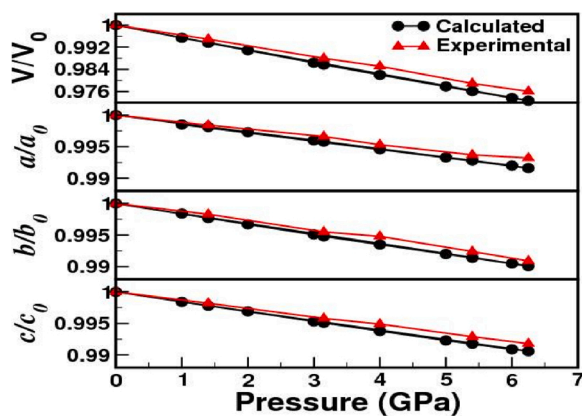


Fig. 3. Experimental [25] and calculated pressure-cell parameters and pressure-volume relation. The error in experimental data is within 0.001–0.003 Å.

Table 2

Comparison between calculated and experimental [25] axial compressibilities.

Axial compressibility ($\times 10^{-3} \text{ GPa}^{-1}$)	Experimental	Calculated
β_a	1.12 (4)	1.31 (1)
β_b	1.46 (5)	1.56 (2)
β_c	1.31 (3)	1.51 (2)

earlier for BeAl_2O_4 [42].

In order to understand the effect of pressure on the structural properties and to relate linear and bulk compressibilities with microscopic properties, we have performed the calculations up to 6 GPa, which is the pressure range of interest for technological applications and the pressure range covered by previous experiments [25]. The occurrence of pressure driven phase transitions, which are expected to happen at higher pressures is beyond the scope of this study. The pressure calculations have been performed using VASP.

Not only unit-cell parameters and volume but also bond lengths, bond angles, and polyhedral volume were calculated at several pressures. Experimental and calculated normalized unit-cell parameters (a/a_0 , b/b_0 , c/c_0) and volume (V/V_0) relations are shown in Fig. 3 (and in more detail in Supplementary information Table ST2). The agreement is excellent. The axial compressibilities are calculated from unit-cell parameters at several pressures. The average axial compressibilities are listed in Table 2, which infers that the difference between the largest and smaller linear compressibility is only 15%. So, it can be concluded that the compression is slightly anisotropic. The behavior of the linear compressibility is $\beta_b > \beta_c > \beta_a$, which is similar to the experimental results [25]. The agreement between experiments and calculations regarding the change with pressure of the crystal structure supports the use of DFT calculations to study the HP behavior of other physical properties.

The anisotropic compressibility of BeAl_2O_4 is related to the way the polyhedra are connected making chains along different axes, which is shown in Fig. 1. It can be expected that AlO_6 octahedron is more compressible than BeO_4 . The average bond distances in AlO_6 and BeO_4 are 1.91 Å and 1.65 Å, respectively, which makes the BeO_4 units more rigid than AlO_6 units (as seen in many oxides). Then volume change will be mainly dominated by reduction of empty space in the structure (by compression and polyhedra tilting) and compression of AlO_6 . Because of the way AlO_6 and BeO_4 are connected, there is empty space along b -axis, which makes it main compressibility axis. To reduce the b -axis is the most efficient way to reduce the volume. As a consequence, b -axis is slightly more compressible than the c -axis, in which compression is determined only by volume decrease of AlO_6 . From the polyhedra Fig. 1,

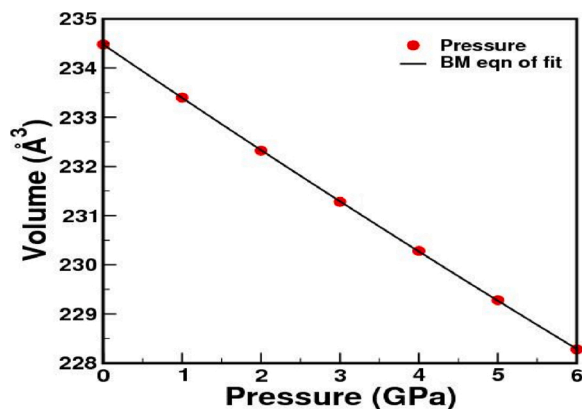


Fig. 4. Unit cell volume of BeAl_2O_4 as a function of pressure.

the linear chain of AlO_6 units along c -axis can be noticed. Along the a -axis, in between the chains of AlO_6 units, there is always a BeO_4 tetrahedron, which reduce the compressibility of a -axis, making it less compressible direction. The Birch-Murnaghan equation of states fit to the pressure-volume results is shown in Fig. 4. The bulk modulus B_0 and the 1st derivative of the B_0 at 0 GPa was found to be 213 GPa and 3.58, respectively. The ambient-pressure volume is 234.48 \AA^3 . The implied value of the 2nd derivative of the B_0 is -0.3889 GPa^{-1} [43]. As described in the introduction, the crystal structure of BeAl_2O_4 is similar to the Spinel structure. Thus, it is reasonable to compare the bulk modulus of both structures. Spinel like MgAl_2O_4 and ZnAl_2O_4 have bulk modulus around 196 GPa [44] and 202 GPa [23], respectively. By comparing with our results, we can state that Chrysoberyl is less compressible than Spinel aluminates. The main reason of it is the smaller volume of the AlO_6 octahedral units in BeAl_2O_4 than in Spinel aluminates. Since most of the volume of the unit-cell of Chrysoberyl and Spinel structures is occupied by the AlO_6 octahedra, these units are expected to dominate compression. By assuming this hypothesis, the bulk modulus of Chrysoberyl and Spinel can be estimated by using the phenomenological relation proposed by Errandonea and Manjon [45] which related the bulk modulus to bond distances. By doing it, bulk modulus of 250 GPa and 200 GPa are obtained for BeAl_2O_4 and Spinel aluminates, respectively; which confirm our conclusion that Chrysoberyl is less compressible Spinel-type aluminates.

A deep understanding of the crystal structure of BeAl_2O_4 at high-pressures can be obtained from the study of the behavior of bond angles, bond lengths, polyhedral volumes, and bond angle variance at high pressures [46]. The results obtained from our study are shown in Fig. 5 (and in more detail in the Supplementary Information Figs. S1, S2, and Tables ST3, ST4, ST5). The ideal tetrahedral angle is 109.5. The Beryllium ions are tetrahedrally coordinated in BeAl_2O_4 . At ambient conditions, the angles of beryllium tetrahedron (O-Be-O) range from 98.27 to 118.6; i.e., an important distortion from ideal tetrahedron is present. Since Al1 and Al2 are nonequivalent, their coordination octahedron and bond angles with oxygen atoms are different. At ambient, the O-Al1-O angles are ranging from 85.76° to 97.36° and O-Al2-O angles are ranging from 79.63° to 100.57°. As can be seen in Fig. S1, under compression, bond angles are not varying significantly. Therefore, tilting of the polyhedral does not play a prominent role in compression of BeAl_2O_4 , which is governed by the reduction of interatomic distances. The calculated bond distances at high-pressure show the similar kind of variation to the experiments, which is shown in Fig. S2 (Sup. Material). In particular, we found that Be-O bonds are as compressible as Al-O bonds contributing to the decrease of the volume of both BeO_4 and AlO_6 polyhedra (shown in Fig. 5) to the volume reduction of BeAl_2O_4 under compression. This explains why the phenomenological model used to compare the bulk modulus of Chrysoberyl with Spinel-type aluminates (which ignores the contribution to BeO_4) slightly

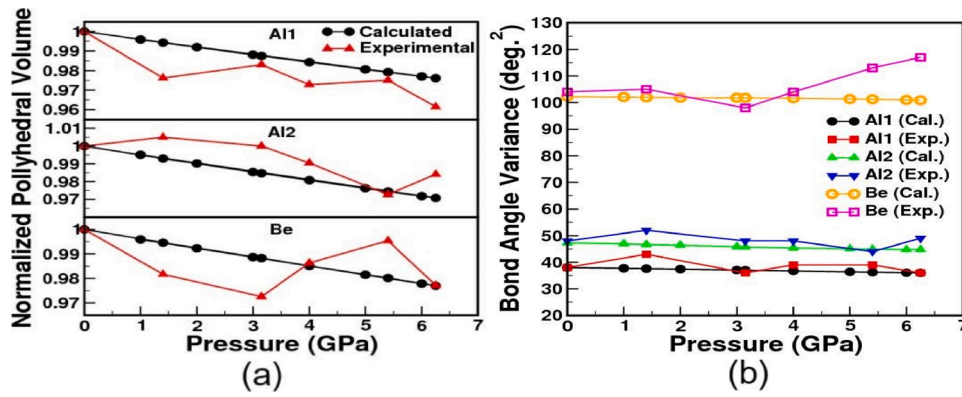


Fig. 5. (a) Octahedron Al1 & Al2 and tetrahedron Be normalized polyhedral volume, (b) bond angle variance at different pressures.

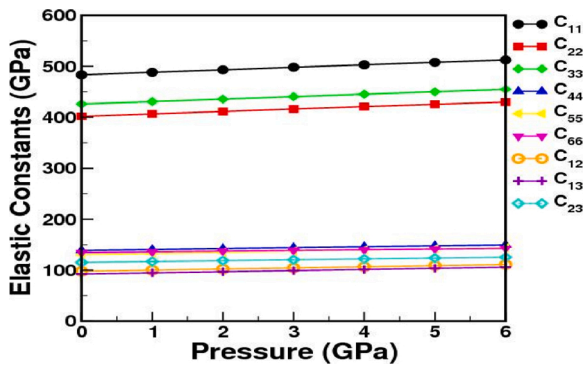


Fig. 6. Calculated elastic constants as a function of pressure.

overestimated the bulk modulus of BeAl_2O_4 . Finally, in Fig. 5, it can be also seen that the bond angle variance is not significantly affected by pressure which indicates that the shape of the polyhedra is not modified up to 6 GPa.

3.2. Elastic and mechanical properties

The elastic constants confer the knowledge of the nature of mechanical properties like stability and under external stresses. The calculation for the elastic constants C_{ij} were performed by the ab-initio technique using the equilibrium cell parameters. The obtained elastic constants fulfill the requirement of being a mechanically stable material [47]. Thus, according to the mechanical stability criteria [48], BeAl_2O_4 was found to be a mechanical stable material. To determine the material's nature at high-pressure, the elastic constants were calculated at ambient and at high-pressure, which is demonstrated in Fig. 6. In this figure, it can be seen that the elastic constant's value increases with

pressure.

By using the elastic constants, the polycrystalline bulk (B) and shear modulus (G) can be calculated. To determine these moduli, two approximation methods were taken into consideration: (a). Voigt method (b). Reuss method [48,49]. According to Hill, the bulk modulus (B) is the arithmetic mean of the Voigt (B_V) and Reuss bulk (B_R). And the shear modulus (G) is of shear moduli (G_V) and (G_R) [50]. The Young's modulus (E) and Poisson's ratio (ν) can be determined in the form of bulk and shear modulus [51,52]. The obtained moduli and Poisson ratio (ν) at different pressures are listed in Table ST6. The obtained bulk modulus at zero pressure is similar to the value of B_0 determined with the BM equation of state. In Fig. 7(a), it can be seen that the calculated value of elastic properties increases with pressure, which means the resistance ability to volume, shape and stiffness of BeAl_2O_4 is increasing with increasing pressure.

Brittleness and ductility are two important mechanical properties of any material. According to Pugh [53], B/G ratio gives the idea about the material's brittle and ductile behavior. The critical value of B/G is 1.75, it separates the material's ductile and brittle behavior. The material exhibits the ductile behavior if B/G ratio is greater than 1.75, otherwise it behaves as a brittle material. The calculated B/G ratio at several pressures for BeAl_2O_4 are listed in TableST6. At ambient pressure the value of B/G is 1.455, which makes it a brittle material. On the other hand, Poisson's ratio is also helpful to provide the knowledge of ductile and brittle behavior of any material. According to Frantsevich [54], if Poisson's ratio (ν) values of any material are less than $1/3$ then it shows brittle nature otherwise it exhibits ductile behavior. In the case of BeAl_2O_4 , we get $\nu = 0.22048$, which means it behaves a brittle material. From the Fig. 7(b), we can see that B/G and Poisson's ratio increases with the pressure ranging from the 0 GPa to 6 GPa, but remains less than 1.75 and $1/3$, respectively. Thus, according to Pugh and Frantsevich's criterion BeAl_2O_4 is a brittle compound. According to Pettifor [55], the nature of the atomic bonding and brittle/ductile nature in compounds

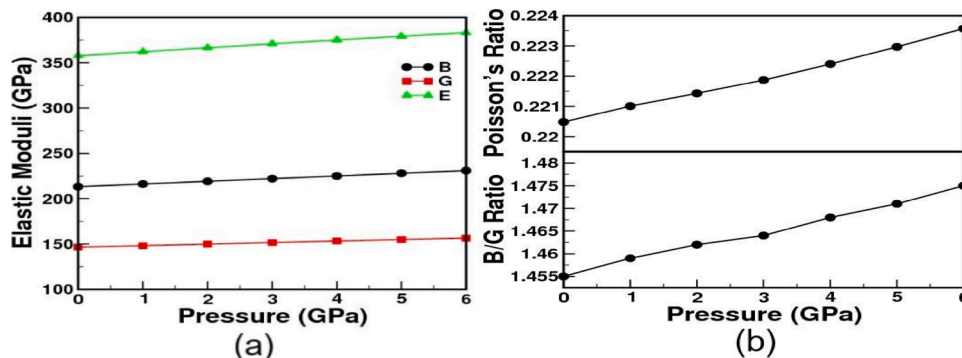


Fig. 7. (a) Bulk modulus (B), Shear modulus (G), Young's modulus (E) and (b) Poisson's ratio (ν), B/G ratio as a function of pressure.

Table 3
The shear anisotropy factors at different pressures (in GPa).

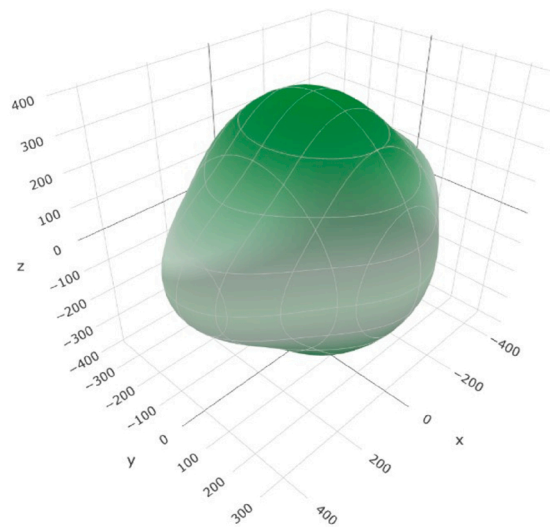
P	A ₁	A ₂	A ₃	A _B (%)	A _G (%)	A ^U
0	0.77	0.87	0.78	0.131×10^{-2}	0.8427×10^{-2}	0.0876
1	0.771	0.880	0.783	0.1317×10^{-2}	0.8060×10^{-2}	0.0839
2	0.776	0.887	0.785	0.1323×10^{-2}	0.7700×10^{-2}	0.0802
3	0.780	0.893	0.787	0.1327×10^{-2}	0.7347×10^{-2}	0.0767
4	0.784	0.899	0.789	0.1332×10^{-2}	0.7072×10^{-2}	0.0739
5	0.788	0.904	0.791	0.1337×10^{-2}	0.6805×10^{-2}	0.0712
6	0.792	0.910	0.793	0.1342×10^{-2}	0.6546×10^{-2}	0.0686

can be revealed by the Cauchy’s pressure, if it is negative then a compound has angular bonds and brittle nature, otherwise the material shows metallic bonding and ductile nature. For the orthorhombic system, the Cauchy’s pressure will be: $C_{23} - C_{44}$ for (100) plane, $C_{13} - C_{55}$ for (010) plane and $C_{12} - C_{66}$ for (001) plane. In the present case of BeAl_2O_4 , the calculated value is -23.42 GPa for $C_{23} - C_{44}$, -37.98 GPa for $C_{13} - C_{55}$ and -36.79 GPa for $C_{12} - C_{66}$. The results show that Cauchy’s pressure values are negative, hence the compound has the angular character of atomic bonding.

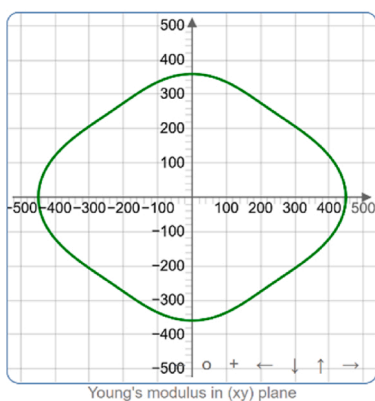
To describe the material’s nature, there are additional physical

parameters, being hardness one of them, probably one of the most important. The material’s hardness depends upon the Young’s modulus and Poisson’s ratio [56]. The obtained hardness of BeAl_2O_4 at several pressures are summarized in Table ST6 (Sup. Material). The hardness of BeAl_2O_4 was studied also the methodology described by Chen [56,57]. According to Chen’s method, the Vickers hardness depends upon the both bulk and shear modulus, which can be determined from Pugh’s modulus ratio [57]. Calculated values of Vickers hardness are shown in Table ST6 (Sup. Material). So, in our study, as the pressure increases, BeAl_2O_4 is becoming harder.

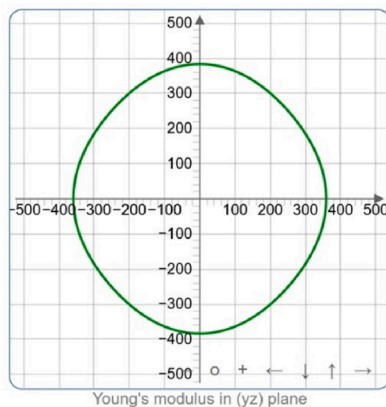
Several crystals, which have low symmetry show high elastic anisotropic degree [58]. The shear anisotropy factors on different crystallographic planes gives the information of the anisotropic degree. The shear anisotropic factors (A_1, A_2, A_3) in atomic bonding for crystallographic planes can be calculated by the elastic constants. If the value of the shear anisotropic factor is unity, then a material shows the isotropic properties [51,59]. On another hand, according to Chung and Buessem [60], the elastic anisotropy can be determined by the anisotropy’s percentage in the bulk (A_B) and shear modulus (A_G). Ranganathan and Ostoja-Starzewski [61] also suggested a universal anisotropy factor (A^U) to observe the anisotropy of the crystal. If A_B, A_G and A^U are



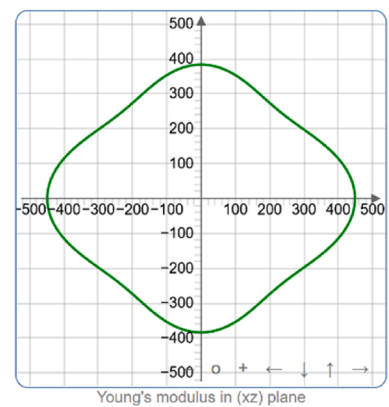
(a)



(b)



(c)



(d)

Fig. 8. The surface contour of the Young’s modulus (a) and plane projections of the Young’s modulus in xy - plane (b), yz - plane (c), xz - plane (d).

Table 4

The density (ρ), longitudinal (v_l), transverse (v_t), average (v_m) elastic wave velocities and Debye temperature (θ_D) at different pressures (P).

P (GPa)	ρ (g/cc)	v_l (km/sec)	v_t (km/sec)	v_m (km/sec)	θ_D (K)
0	3.5962	10.6605	6.3836	7.0632	1035.85
1	3.6129	10.7020	6.4046	7.0868	1040.92
2	3.6293	10.747	6.429	7.1141	1046.52
3	3.6458	10.7917	6.4519	7.1399	1051.90
4	3.6619	10.8329	6.4727	7.1632	1056.88
5	3.6780	10.8731	6.4923	7.1855	1061.71
6	3.6937	10.9118	6.5109	7.2065	1066.35

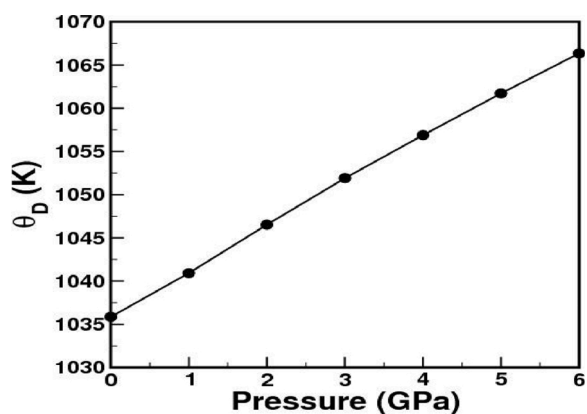


Fig. 9. Debye temperature as a function of pressure.

zero then the crystal will exhibit isotropic nature. In the present case, A_1 , A_2 and A_3 for $\{100\}$, $\{010\}$ and $\{001\}$, respectively, A_B , A_G and A^U at high-pressure are listed in Table 3. The calculated value of A_1 , A_2 and A_3 increases as the pressure increases and it is moving towards unity. So, we can say that the BeAl_2O_4 shows the nearly isotropic behavior. The values of A_G , A_B and A^U are close to zero and decreasing with increasing the pressure, which makes it nearly isotropic material. The calculated values of A_G as a function of pressure are larger than A_B , which means that the shear modulus is a stronger direction dependent than the bulk modulus. In addition, three- and two-dimensional Young modulus at ambient pressure are shown in Fig. 8. Material's isotropic nature can be understood by Young modulus. If Young modulus surface is spherical then material shows isotropic nature [62,63]. From the plots, it can be seen that the Young modulus surface is nearly spherical along yz - plane which emphasizes the nearly isotropic nature.

The sound velocities can be obtained from the elastic constants. The longitudinal (v_l), transverse (v_t) and averaged sound velocity (v_m) at high-pressure were calculated by using Navier's equation [50,64,65]. The calculated value increases with pressure, which is given in Table 4. The Debye temperature is an important quantity. It is proportional to the

averaged sound velocities. Using Debye-Grunesien model [50,64,65], obtained Debye temperature as a function of pressure are summarized in Table 4. The variation of Debye temperature at high-pressure is shown in Fig. 9, which increases as the pressure increases.

3.3. Lattice dynamics and thermodynamic properties

In order to investigate the dynamical stability, the phonon dispersion has been calculated and the same is plotted along the high symmetric path ($\Gamma-X-S-Y-\Gamma-Z-U-R-T-Z$) at zero pressure. We found that acoustic branches lie within positive frequency region, implying the dynamical stability of BeAl_2O_4 . The acoustic modes are highly interacting with optical modes. The equivalent atomic masses of entities are responsible for the same and the phonon dispersion curve is shown in Fig. 10. To understand more about the atomic contribution to phonons, we have calculated the phonon density of states. From the plot, it infers that the low-frequency phonon modes are dominating by Be and O atoms. The optical modes positioned at higher frequencies are equally contributed by Al, Be and O atoms. The phonon density of states is also evident for phonon-phonon interactions seen from the phonon dispersion.

The thermodynamic properties are calculated with Phonopy code. It is based on the quasi-harmonic approximation [35]. The calculated thermodynamic properties like bulk modulus, thermal expansion coefficients, volume expansion, specific heat at constant pressure, specific heat at constant volume, entropy, Gibbs free energy, Gruneisen parameter and free energy at high-temperatures are shown in Fig. 11. The variation of the bulk modulus with temperature is shown in Fig. 11(a). From the Fig. 11(a), it can be seen that the bulk modulus decreases with increase in temperature. The low bulk modulus indicates that the material shows compressible nature. The thermal expansion as a function of temperature as shown in Fig. 11(b) reveals the positive thermal expansion coefficient present in the system. Experimental and calculated normalized volume expansion are shown in Fig. 11(c). The specific heat capacity is the measurement of any substance to store the heat. Calculated C_p , C_v and entropy at high-temperatures are shown in Fig. 11(d). From the Fig. 11(d), we can see that at 0 K the entropy is zero and it increases rapidly as the temperature increases. The values of specific heat at constant pressure and at constant volume as a function of temperature are almost similar, which can be seen from the Fig. 11(d). At low temperatures the specific heat increases rapidly, but at high temperatures the variation is small. We can see that at high temperatures the specific heat at constant volume obeys the Dulong-Petit law. The variation of the Gibbs free energy with high-temperature is given in Fig. 11(e), which decreases as the temperature increases. Gruneisen parameters as a function of temperature is shown in Fig. 11(f) and it can be seen that it is positive at each temperature. The relation between the free energy and temperatures are shown in Fig. 11(g). It shows same behavior as Gibbs free energy.

To provide the description of the vibrational modes, the vibrational

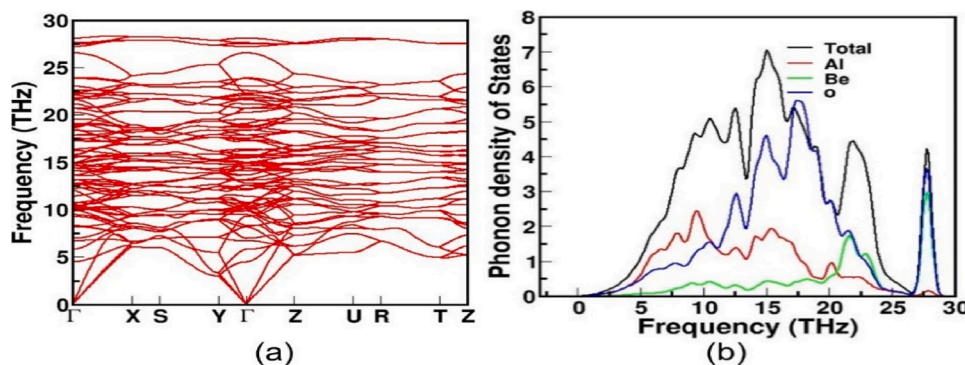


Fig. 10. Phonon dispersion curve for BeAl_2O_4 .

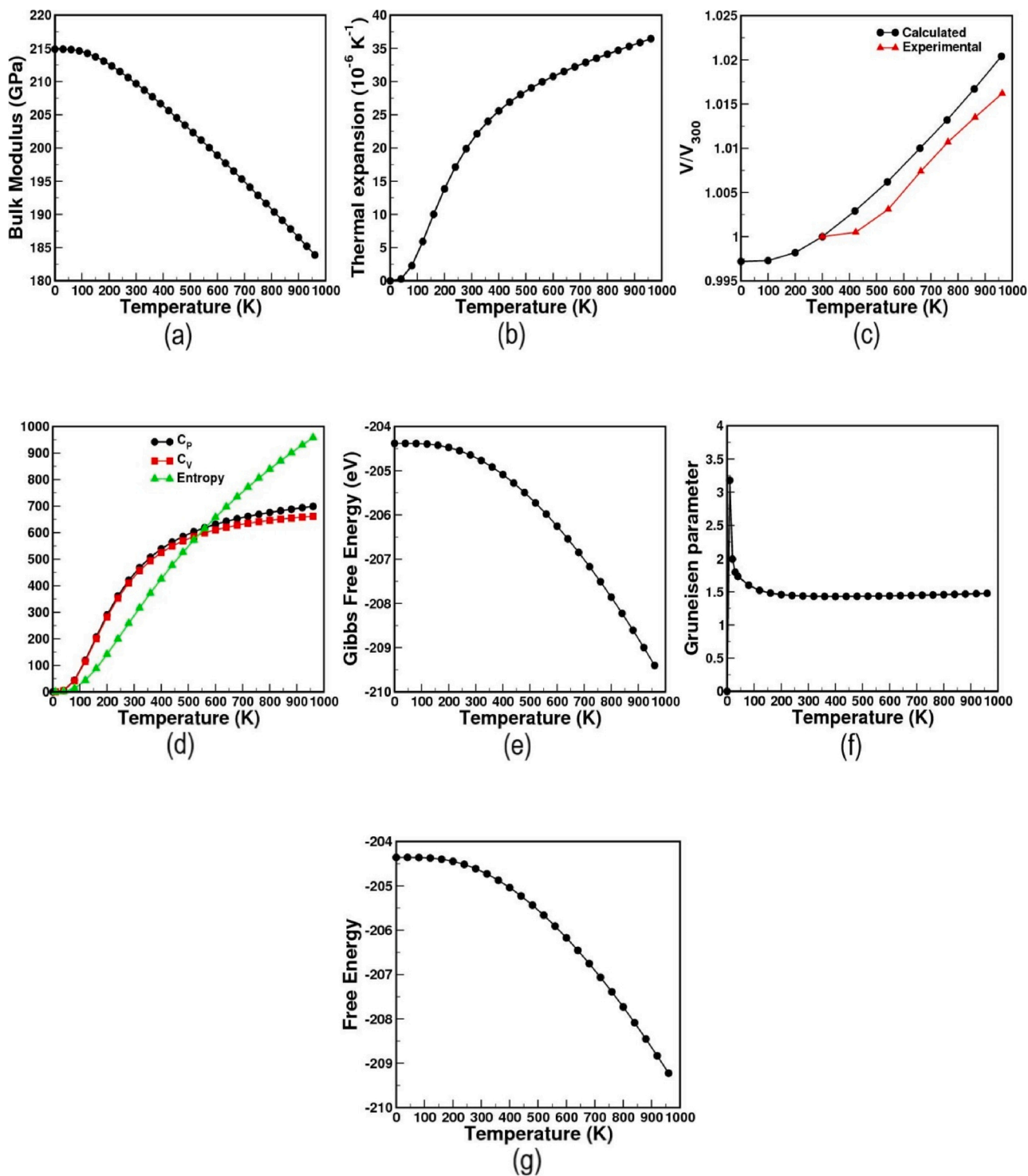


Fig. 11. Bulk modulus, thermal expansion, volume expansion, C_p , C_v , entropy, Gibbs free energy, Gruneisen parameter and free energy as a function of temperature.

properties have been calculated using CASTEP [38]. From the data, it is evident that there are 84 vibrational bands, which are found to agree with the experimental results [66]. The calculated vibrational modes (optical modes) of chrysoberyl are listed in Table ST4 (Sup. Material). Three acoustic modes are $B_{1u} + B_{2u} + B_{3u}$ and the remaining $11A_g + 10A_u + 7B_{1g} + 13B_{1u} + 11B_{2g} + 9B_{2u} + 7B_{3g} + 13B_{3u}$ are optical modes. From the Table ST4 (Sup. Material), it can be seen that optical branches contain 36 Raman active, 35 IR active and 10 silent modes. 36 modes are Raman active, which are $11A_g + 7B_{1g} + 11B_{2g} + 7B_{3g}$. Total number of IR active modes are $13B_{1u} + 9B_{2u} + 13B_{3u}$. The $10A_u$ modes are silent

modes. The calculated Raman modes agree with experiment and the deviation is within 0.07–5.48 %. In addition, there is a particular mode 11 (B_{2g} with 310.91 cm^{-1} frequency) with a larger discrepancy. Regarding IR modes, we would like to state that, we have not included the LO-TO splitting in the calculations, which might result in only fair agreement with the experimental results as far as IR modes are concerned. But in general, the calculated frequencies, usually are closer to the LO mode than to the TO mode, which is seen in the present case also as expected. According to our calculations two modes assigned as IR in the experiments (modes 10 and 55) are indeed silent modes which could

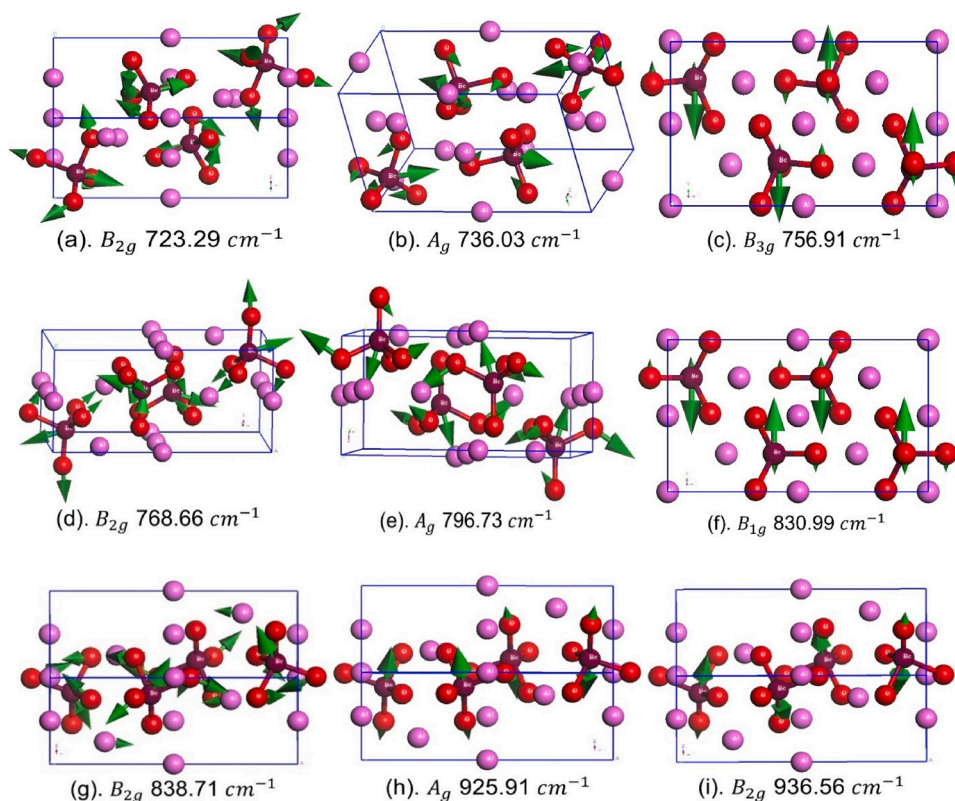


Fig. 12. Raman modes for BeAl_2O_4 at several frequencies.

become active because of the presence of defects in the crystal [67]. Raman modes at above 700 cm^{-1} frequencies are shown in Fig. 12. Raman mode at 723.29 cm^{-1} frequency is due to the stretching and scissoring in BeO_4 . AlO_6 has larger bond distance than BeO_4 , which makes it less interactive at high frequencies. From the Fig. 12(a) it can be seen that there is no motion in Al units. Fig. 12(b) represents the Raman mode at 736.03 cm^{-1} , which is due to the scissoring in BeO_4 . Generally, symmetry stretching vibrations considered to be Raman active modes but mode at 756.91 cm^{-1} represents the asymmetric stretching in BeO_4 , which is shown in Fig. 12(c). The mode at 768.66 cm^{-1} (in Fig. 12(d)) has the scissoring, stretching and rocking vibrations in BeO_4 . Fig. 12(e) shows the Raman mode at 796.73 cm^{-1} which is having scissoring and wagging vibrations in BeO_4 . Fig. 12(f) represents the asymmetric stretching vibration in BeO_4 at 830.99 cm^{-1} frequency. Due to the large bond distances in AlO_6 , it is not much active at high frequencies, mode at 838.71 cm^{-1} includes vibration in BeO_4 as well as AlO_6 . It has scissoring

vibration in BeO_4 and stretching of Al-O bond, which is shown in Fig. 12 (g). From the Fig. 12(g), it can be stated that the vibrations are highly contributed by BeO_4 . The modes at 925.91 cm^{-1} and 936.56 cm^{-1} are having both asymmetric and symmetric stretching vibrations in BeO_4 , which can be seen in Fig. 12(h) and (i), respectively.

3.4. Electronic structure and optical properties

Finally, in order to determine the full description of the physical properties of BeAl_2O_4 , electronic structure calculations have been performed using GGA-PBE functional. The obtained band gap is 6.0 eV . It is well understood that GGA underestimated the band gap of insulators/semiconductors, thus in order to improve the band gap description, the employment of TB-mBJ functional has been done on our self-consistent ground state properties. The obtained band gap is found to be around 8.3 eV , which is represented in Fig. 13(a). The band gap is found to be in

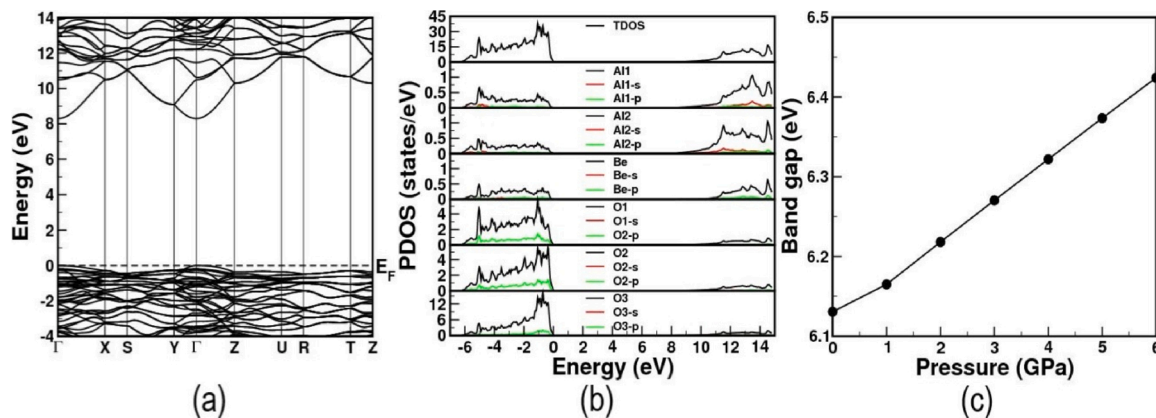


Fig. 13. Electronic structure (a), PDOS (b) and band gap variation (c) of BeAl_2O_4 .

good agreement with recent study by Y. Wang et al. [29]. By observing the band structure, it can be said that the investigated system is a direct gap insulator since the top of the valence band and bottom of the conduction band are both situated at the center of the Brillouin zone, i.e. Γ point. In addition, it is found that the dispersion of the valence band is small, but the conduction band is highly dispersive. The detailed analysis of the electronic structure properties can be understood through the total and partial electronic density of states (DOS) which are plotted in Fig. 13(b). From the plots, it can be seen that the valence bands are predominantly dominated by O ($2p$) orbitals and the conduction bands are mainly dominated by Al ($3s$). From the Fig. 13(b), it can be said that the partial density of states of Be, Al1 and Al2 are quietly similar with each other. The partial DOS (PDOS) of different oxygen atoms are quite different with each other. This is related to their different bonding. The bonding of O1 and O2 with Be and Al are same. In contrast, O3 shows different bonding behavior with Be and Al. All oxygens are connected to one beryllium and three aluminum ions. O1 and O2 each have two Al1 and one Al2, but O3 is linked to two Al2 and one Al1. As a consequence, O3 shows large contribution in valence band rather than O1 and O2.

To analyze the electronic properties under pressure, high pressure calculations were carried out. The pressure calculations have been performed by using VASP with PBE-GGA exchange correlation functional. This method, in spite of underestimating the value of the band-gap, gives an accurate description of its pressure dependence and it is much less demanding of computing resources than the TB-mBJ method used for the ambient-pressure calculations. The band gap is found to increase with pressure, and the variation is shown in Fig. 13(c). This is outcome of the enhancement under compression of the repulsion between bonding and antibonding states near the Fermi level, caused by the compression of AlO_6 octahedral units [68].

In order to obtain further information, the optical properties of BeAl_2O_4 have been determined using TB-mBJ functional with dense k -mesh of $50 \times 23 \times 41$. In Fig. S3 (Sup. Material), the real and imaginary parts of the dielectric function are displayed. The imaginary part of the dielectric function contains the information about the transition mechanism. By using Kramers-Kronig relations, the real part of the dielectric function can be determined from the imaginary part. The optical properties like reflectivity and absorptivity can be calculated through the imaginary part of dielectric function. From the absorptivity plots, it can be said that the absorption edge is equal to its band gap. The transition is beginning after the photon energy 8.3 eV. The static refractive index is approximately 1.2, which is nearly the same in all crystallographic directions. This is evident for nearly optical isotropic nature in the present investigated system. The investigated system is optically isotropic, the refractive index in low photon energy range is evident for it. This investigated system can be good for UV applications, the absorption spectra is evident for it.

4. Conclusion

In summary, the structural, electronic, optical, elastic, vibrational, and mechanical properties of BeAl_2O_4 have been studied using density-functional theory. Calculations give an accurate description of the crystal structure and its HP behavior. They also help to deepen the understanding of the properties of BeAl_2O_4 . It is also found that Chrysoberyl exhibits mechanical and dynamical stability and it is identified as a large gap insulator with a direct band gap of around 8.3 eV. The calculated structural and electronic structural properties are found to agree with the experiments. The description of the pressure behavior is quite accurate. From the elastic properties results of BeAl_2O_4 , it is confirmed that chrysoberyl, in contrast to other Olivine-type oxides, shows nearly isotropic compressibility. It has a 213 GPa as bulk modulus, which makes it less compressible than the other Olivine-type and Spinel-type related compounds and has 20–27 GPa hardness, which makes it an extremely hard material. This fact is related to the presence of one of small AlO_6 octahedral units. According to the Pugh

and Frantsevich criteria BeAl_2O_4 is a brittle material. The pressure studies infer that the band gap increases with increasing the pressure due to the enhancement of the repulsion between bonding and antibonding states. The structural parameters under pressure are found in good accord with the experiments. The optical properties at ambient reflect the nearly isotropic properties.

CRedit authorship contribution statement

Jaspreet Singh: Executing the problem, Running the calculations, Data Analysis, Manuscript preparation. **Vineet Kumar Sharma:** Running a part of the program, Discussion of results, Analysis, Manuscript editing. **VK:** Problem Identification, Data Analysis, Discussion of Results, Manuscript Preparation and editing, Funding, Supervision, acquisition, writing-original draft. **G Vaitheeswaran:** Conceptualization, investigation, methodology. **D Errandonea:** Validation, Visualization, Writing - review and editing.

Declaration of Competing Interest

The authors declare that they have no known competing financial interests or personal relationships that could have appeared to influence the work reported in this paper.

Acknowledgments

Jaspreet Singh, VKS and VK would like to acknowledge IIT Hyderabad for computational facility. Jaspreet Singh would like to acknowledge CSIR for the fellowship and VKS also would like to acknowledge MHRD for fellowship.

D. E. acknowledges financial support given by the Spanish Ministry of Science, Innovation and Universities under Grant Nos. PID2019-106383GB-C41 and RED2018-102612-T (MALTA Consolider-Team network) and by Generalitat Valenciana under Grant Prometeo/2018/123 (EFIMAT), and the technical assistance provided by the Tirant III facility at University of Valencia.

G. V. acknowledges, CMSD, University of Hyderabad for providing computational facility.

Jaspreet Singh would like to acknowledge Subrata Mondal, University of Hyderabad for fruitful discussion on vibrational properties analysis.

Appendix A. Supplementary data

Supplementary material related to this article can be found, in the online version, at doi:<https://doi.org/10.1016/j.mtcomm.2020.101801>.

References

- [1] W.L. Bragg, G.B. Brown, XXX. Die Struktur des Olivins, *Zeitschrift für Kristallographie-Crystalline Materials* 63 (1926) 538–556.
- [2] E.F. Farrell, J.H. Fang, R.E. Newham, Refinement of the chrysoberyl structure, *Am. Mineral.* 48 (1963) 804–810.
- [3] Devin Pugh-Thomas, Brian M. Walsh, Mool C. Gupta, Spectroscopy of $\text{BeAl}_2\text{O}_4:\text{Cr}^{3+}$ with application to high-temperature sensing, *Appl. Opt.* 49 (2010) 2891–2897.
- [4] Jingqing Liu, et al., The ayalitence spectrum of chrysoberyl $\text{BeAl}_2\text{O}_4:\text{Cr}^{3+}$ at high pressure and low temperature, *J. Lumin.* 40 (1988) 419–420.
- [5] J.C. Walling, et al., Tunable alexandrite lasers, *IEEE J. Quantum Electron.* 16 (1980) 1302–1315.
- [6] William Lawrence Bragg, G. Burniston Brown, The crystalline structure of chrysoberyl, *Proc. Royal Soc. London. Series A* 110 (1926) 34–63.
- [7] Hill, Monk Reginald. Method of improving the brilliance and color of titanium dioxide. U.S. Patent No. 2,304,947 (1942).
- [8] T. Pilati, et al., Atomic thermal parameters and thermodynamic functions for chrysoberyl (BeAl_2O_4) from vibrational spectra and transfer of empirical force fields, *Acta Crystallogr., B* 49 (1993) 216–222.
- [9] E.F. Farrell, J.H. Fang, Flux growth of chrysoberyl and alexandrite, *J. Am. Ceram. Soc.* 47 (1964) 274–276.

- [10] Dibyendu Ganguli, Prasenjit Saha, Preliminary investigations in the High-Silica region of the system $\text{BeO-Al}_2\text{O}_3\text{-SiO}_2$, *Trans. Indian Ceram. Soc.* 24 (1965) 134–146.
- [11] Dibyendu Ganguli, Prasenjit Saha, A reconnaissance of the system $\text{BeO-Al}_2\text{O}_3\text{-SiO}_2\text{-H}_2\text{O}$, *Trans. Indian Ceram. Soc.* 26 (1967) 102–110.
- [12] Raj Kumar Verma, Elasticity of some high-density crystals, *J. Geophys. Res.* 65 (1960) 757–766.
- [13] Mineo Kumazawa, Orson L. Anderson, Elastic moduli, pressure derivatives, and temperature derivatives of single-crystal Olivine and single-crystal forsterite, *J. Geophys. Res.* 74 (1969) 5961–5972.
- [14] Shukusuké Kōzu, Jun-ichi Ueda, Shizuo Tsurumi, Thermal expansion of Olivine, *Proc. Imp. Acad.* 10 (1934) 83–86.
- [15] Naohiro Soga, O. rson L. Anderson, High-temperature elasticity and expansivity of forsterite and steatite, *J. Am. Ceram. Soc.* 50 (1967) 239–242.
- [16] Robert M. Hazen, Effects of temperature and pressure on the crystal structure of forsterite, *Am. Mineral.* 61 (1976) 1280–1293.
- [17] Yasuhiro Kudoh, Yoshio Takéuchi, The crystal structure of forsterite Mg_2SiO_4 under high pressure up to 149 kb, *Zeitschrift für Kristallographie-Crystalline Materials* 171 (1985) 291–302.
- [18] Robert M. Hazen, Effects of temperature and pressure on the crystal structure of ferromagnesian Olivine, *Am. Mineral.* 62 (1977) 286–295.
- [19] Y. Kudoh, H. Takeda, Single crystal X-ray diffraction study on the bond compressibility of Fayalite, Fe_2SiO_4 and rutile, TiO_2 under high pressure, *Physica B + C* 139 (1986) 333–336.
- [20] Z.D. Sharp, R.M. Hazen, L.W. Finger, High-pressure crystal chemistry of monticellite, CaMgSiO_4 , *Am. Mineral.* 72 (1987) 748–755.
- [21] W.A. Dollase, A method of determining the distortion of coordination polyhedra, *Acta Crystallogr. A* 30 (1974) 513–517.
- [22] Sinhué López-Moreno, et al., Lattice dynamics of ZnAl_2O_4 and ZnGa_2O_4 under high pressure, *Ann. Phys.* 523 (2011) 157–167.
- [23] Davide Levy, et al., Structure and compressibility of synthetic ZnAl_2O_4 (gahnite) under high-pressure conditions, from synchrotron X-ray powder diffraction, *Phys. Chem. Miner.* 28 (2001) 612–618.
- [24] D. Santamaría-Pérez, et al., Crystal structure of sinhalite MgAlBO_4 under high pressure, *J. Phys. Chem. C* 119 (2015) 6777–6784.
- [25] Robert M. Hazen, High-pressure crystal chemistry of chrysoberyl, Al_2BeO_4 : insights on the origin of Olivine elastic anisotropy, *Phys. Chem. Miner.* 14 (1987) 13–20.
- [26] W.Y. Ching, Yong-Nian Xu, B.K. Briceken, Comparative study of the electronic structure of two laser crystals: BeAl_2O_4 and LiYF_4 , *Phys. Rev. B* 63 (2001) 115101.
- [27] A.H. Jahren, M.B. Kruger, Raymond Jeanloz, Alexandrite as a high-temperature pressure calibrant, and implications for the ruby-fluorescence scale, *J. Appl. Phys.* 71 (1992) 1579–1582.
- [28] D. Tromans, J.A. Meech, Fracture toughness and surface energies of minerals: theoretical estimates for oxides, sulphides, silicates and halides, *Miner. Eng.* 15 (2002) 1027–1041.
- [29] Y. Wang, et al., High-throughput first-principles calculations as a powerful guiding tool for materials engineering: case study of the AB_2X_4 (A = Be, Mg, Ca, Sr, Ba; B = Al, Ga, In; X = O, S) spinel compounds, *Results Phys.* 13 (2019), 102180.
- [30] A. Benmakhlof, et al., New pressure-induced polymorphic transitions of anhydrous magnesium sulfate, *J. Chem. Soc. Dalton Trans.* 46 (2017) 5058–5068.
- [31] Georg Kresse, Jürgen Furthmüller, Efficiency of ab-initio total energy calculations for metals and semiconductors using a plane-wave basis set, *Comput. Mater. Sci.* 6 (1996) 15–50.
- [32] John P. Perdew, Kieron Burke, Matthias Ernzerhof, Generalized gradient approximation made simple, *Phys. Rev. Lett.* 77 (1996) 3865.
- [33] Hendrik J. Monkhorst, James D. Pack, Special points for Brillouin-zone integrations, *Phys. Rev. B* 13 (1976) 5188.
- [34] Xavier Gonze, Changyol Lee, Dynamical matrices, born effective charges, dielectric permittivity tensors, and interatomic force constants from density-functional perturbation theory, *Phys. Rev. B* 55 (1997) 10355.
- [35] Romain Gaillac, Pluton Pullumbi, François-Xavier Coudert, ELATE: an open-source online application for analysis and visualization of elastic tensors, *J. Phys. Condens. Matter* 28 (2016), 275201.
- [36] Atsushi Togo, et al., First-principles phonon calculations of thermal expansion in Ti_3SiC_2 , Ti_3AlC_2 , and Ti_3GeC_2 , *Phys. Rev. B* 81 (2010), 174301.
- [37] Daniel Errandonea, et al., Theoretical and experimental study of the crystal structures, lattice vibrations, and band structures of monazite-type PbCrO_4 , PbSeO_4 , SrCrO_4 , and SrSeO_4 , *Inorg. Chem.* 54 (2015) 7524–7535.
- [38] Peter Blaha, et al., Full-potential, linearized augmented plane wave programs for crystalline systems, *Comput. Phys. Commun.* 59 (1990) 399–415.
- [39] S.J. Clark, M.D. Segall, C.J. Pickard, P.J. Hasnip, M.J. Probert, K. Refson, M. C. Payne, *Z. Für Krist.* 220 (2005) 567–570.
- [40] Francis Birch, Finite elastic strain of cubic crystals, *Phys. Rev.* 71 (1947) 809.
- [41] J.C. Walling, et al., Tunable alexandrite lasers, *IEEE J. Quantum Electron.* 16 (1980) 1302–1315.
- [42] Kai Wang, et al., First-principles study on magnetoelectric coupling effect of M/BiFeO_3 (M = Co, Fe) multiferroic superlattice, *Vacuum* 165 (2019) 105–112.
- [43] D. Errandonea, et al., High-pressure x-ray diffraction and ab initio study of $\text{Ni}_2\text{Mo}_3\text{N}$, $\text{Pd}_2\text{Mo}_3\text{N}$, $\text{Pt}_2\text{Mo}_3\text{N}$, $\text{Co}_3\text{Mo}_3\text{N}$, and $\text{Fe}_3\text{Mo}_3\text{N}$: two families of ultra-incompressible bimetallic interstitial nitrides, *Phys. Rev. B* 82 (2010), 174105.
- [44] M.B. Kruger, et al., Equation of state of MgAl_2O_4 spinel to 65 GPa, *Phys. Rev. B* 56 (1997) 1.
- [45] Daniel Errandonea, Francisco Javier Manjon, Pressure effects on the structural and electronic properties of ABX_4 scintillating crystals, *Prog. Mater. Sci.* 53 (2008) 711–773.
- [46] Daniel Errandonea, et al., High-pressure crystal structure, lattice vibrations, and band structure of BiSbO_4 , *Inorg. Chem.* 55 (2016) 4958–4969.
- [47] Félix Mouhat, François-Xavier Coudert, Necessary and sufficient elastic stability conditions in various crystal systems, *Phys. Rev. B* 90 (2014) 224104.
- [48] Friedrich Wille, *Die Mathematik im Verlag BG Teubner, Wechselwirkungen.* Vieweg+ Teubner Verlag, Wiesbaden, 1986, pp. 27–72.
- [49] A. Reuss, Berechnung der Fliegrenze von Mischkristallen auf Grund der Plastizitätsbedingung für Einkristalle, *Z. Angew. Math. Mech.* 9 (1929) 49–58.
- [50] Richard Hill, The elastic behaviour of a crystalline aggregate, *Proc. Phys. Soc. Sect. A* 65 (1952) 349.
- [51] P. Ravindran, et al., Density functional theory for calculation of elastic properties of orthorhombic crystals: application to TiSi_2 , *J. Appl. Phys.* 84 (1998) 4891–4904.
- [52] K.B. Panda, K.S. Ravi Chandran, First principles determination of elastic constants and chemical bonding of titanium boride (TiB) on the basis of density functional theory, *Acta Mater.* 54 (2006) 1641–1657.
- [53] S.F. Pugh, XCII. Relations between the Elastic Moduli and the Plastic Properties of Polycrystalline Pure Metals, *The London, Edinburgh, and Dublin Philosophical Magazine and Journal of Science*, 1954, pp. 823–843.
- [54] I.N. Frantsevich, F. F. Voronov, S.A. Bokuta, in: I.N. Frantsevich (Ed.), *Elastic Constants and Elastic Moduli of Metals and Insulators Handbook*, Naukova Dumka, Kiev, 1983, p. 60.
- [55] D.G. Pettifor, Theoretical predictions of structure and related properties of intermetallics, *Mater. Sci. Technol.* 8 (1992) 345–349.
- [56] Hsien-Chie Cheng, Ching-Feng Yu, Wen-Hwa Chen, First-principles density functional calculation of mechanical, thermodynamic and electronic properties of CuIn and Cu_2In crystals, *J. Alloys. Compd.* 546 (2013) 286–295.
- [57] Xing-Qiu Chen, et al., Modeling hardness of polycrystalline materials and bulk metallic glasses, *Intermetallics* 19 (2011) 1275–1281.
- [58] Viggo Tvergaard, John W. Hutchinson, Microcracking in ceramics induced by thermal expansion or elastic anisotropy, *J. Am. Ceram. Soc.* 71 (1988) 157–166.
- [59] B. Xiao, et al., Mechanical properties and chemical bonding characteristics of Cr_7C_3 type multicomponent carbides, *J. Appl. Phys.* 109 (2011), 023507.
- [60] D.H. Chung, W.R. Buessem, The elastic anisotropy of crystals, *J. Appl. Phys.* 38 (1967) 2010–2012.
- [61] Shivakumar I. Ranganathan, Martin Ostoja-Starzewski, Universal elastic anisotropy index, *Phys. Rev. Lett.* 101 (2008), 055504.
- [62] Chuang Wu, et al., Band Structures, Magnetism, Half-metallicity and Elastic Properties of Full-Heusler Alloy Cr_2Vsb , *J. Phys. Soc. Jpn.* 89 (2020), 064713.
- [63] C. Wu, et al., The structural, half-metal, magnetic, and mechanical properties of full Heusler alloy CrCoVSb : a first-principles study, *Chinese J. Phys.* (2020).
- [64] M.G. Brik, First-principles calculations of electronic, optical and elastic properties of ZnAl_2S_4 and ZnGa_2O_4 , *J. Phys. Chem. Solids* 71 (2010) 1435–1442.
- [65] Yingchun Ding, Theoretical study on stability, mechanical properties and thermodynamic parameters of the orthorhombic- $\text{A}_2\text{N}_2\text{O}$ (A = C, Si and Ge), *Physica B Condens. Matter* 407 (2012) 2190–2200.
- [66] Z. Burshtein, et al., Vibrational spectra of chrysoberyl (BeAl_2O_4), *J. Phys. Chem. Solids* 50 (1989) 1095–1100.
- [67] F.J. Manjón, et al., Silent Raman modes in zinc oxide and related nitrides, *J. Appl. Phys.* 97 (2005), 053516.
- [68] P. Botella, D. Errandonea, A.B. Garg, P. Rodriguez-Hernandez, A. Muñoz, S. N. Achary, A. Vomiero, High-pressure characterization of the optical and electronic properties of InVO_4 , InNbO_4 , and InTaO_4 , *SN Applied Sciences* 1 (2019) 389.